

Submitted to *Frontiers in Fractal Physiology*, special issue on “*Critical Brain Dynamics*”
(Edited by He BY, Daffertshofer A, Boonstra TW)

Avalanche analysis from multi-electrode ensemble recordings in cat, monkey and human cerebral cortex during wakefulness and sleep

Nima Dehghani^{1,*}, Nicholas G. Hatsopoulos², Zach D. Haga², Eric Halgren³, Sydney S. Cash⁴, Alain Destexhe^{1,*}

1 Laboratory of Computational Neuroscience. Unité de Neurosciences, Information et Complexité (UNIC). CNRS. Gif-sur-Yvette, France.

2 Committee on Computational Neuroscience and Department of Organismal Biology and Anatomy, University of Chicago, Chicago, Illinois, USA.

3 Multimodal Imaging Laboratory, Departments of Neurosciences and Radiology, University of California San Diego, La Jolla, CA, USA.

4 Department of Neurology, Massachusetts General Hospital and Harvard Med. School, Boston, MA, USA.

* E-mail: dehghani@unic.cnrs-gif.fr, destexhe@unic.cnrs-gif.fr

Abstract

Self-organized critical states are found in many natural systems, from earthquakes to forest fires, they have also been found in neural systems, particularly, in slice preparations or neuronal cultures. However, the presence of critical states in the awake brain remains controversial. Here, we compared avalanche analyses performed on different *in vivo* preparations during wakefulness and sleep states, in cat parietal cortex (8 electrodes), monkey motor cortex (64/96 electrodes, and in some cases, dual recordings from two cortical areas) and human temporal cortex (96 electrodes) in epileptic patients. In neuronal avalanches defined from units (up to 152 discriminated single units), the size of avalanches never clearly scaled as power-law, but rather scaled exponentially or displayed intermediate scaling. We also analyzed the dynamics of local field potentials (LFPs) and in particular LFP negative peaks (nLFPs) among the different electrodes (up to 96 sites in temporal or motor cortex or up to total of 128 sites in adjacent motor and pre-motor cortices). In this case, the avalanches defined from nLFPs displayed power-law scaling in double logarithmic representations, as reported previously in monkey. However, avalanche defined as positive LFP (pLFP) peaks, which are not related to neuronal firing, also displayed the same apparent power-law scaling. Closer examination of this scaling using the more reliable cumulative distribution function (CDF) and other rigorous statistical measures, showed that avalanche sizes are very unlikely to be power-law distributed. The same pattern was seen for cats, monkey and human, as well as for different brain states, such as wakefulness, slow-wave sleep and REM sleep. We also tested exponential distributions as alternative fits. While simple exponentials yielded very good approximations of the avalanche dynamics, the “sum of exponentials” provided the best fit to the data. Collectively, these results show no clear evidence for power-law scaling or self-organized critical states in the awake and sleeping brain of mammals, from cat to man. The power-law scaling of LFP peaks was only apparent in logarithmic representations, suggesting that such representations cannot be used by themselves to demonstrate the presence of critical dynamics in brain activity.

keywords

Criticality, Self-organization, Brain Dynamics, Scale invariance, Complexity, Power-law

Introduction

Self-organized criticality (SOC) is a dynamical state of a system which maintains itself at (or close to) a phase transition point. This family of systems were initially described work by Bak, Tang and Wiesenfeld (1987), and have been found in many natural systems (reviewed in Bak, 1996; Jensen, 1998). SOC systems are characterized by scale invariance, which is usually identified as a power-law distribution of characteristics of the system’s dynamics such as event size or the waiting time between events. The temporal fingerprint of SOC systems is often $1/f$ noise (“pink” or “flicker” noise). These features are interesting because they show the presence of long-lasting or long-range correlations in the system.

The dynamics of SOC systems is structured as “avalanches” of activity, separated by silent periods. The avalanche sizes are typically distributed as a power law, where the probability of occurrence $p(x)$ of a given avalanche size x scales as:

$$p(x) \sim x^{-\alpha} ,$$

where α is the scaling exponent of the distribution.

SOC systems have been observed in many different natural phenomena, from sandpiles, to rice piles, in forest fires and earthquakes (Frette, 1996; Malamud et al., 1998; Bak, 1996; Jensen 1998, Peters 2006). The presence of SOC was also demonstrated in circuits of neurons *in vitro* (Beggs and Plenz, 2003), where network activity was found to alternate between active and quiescent periods, forming “neuronal avalanches”. The presence of avalanches, although clear *in vitro*, is more controversial *in vivo*. Since power-laws fit neuronal avalanches better than other alternative probability distributions (Klaus and Plenz, 2011), their presence has been taken as evidence for neuronal avalanches *in vivo*. In anesthetized cats (Hahn et al., 2010) and monkeys (Peterman et al., 2009), power-law distributed avalanches have been found in the peaks of local field potentials (LFP). However, LFP peaks are only indirectly related to neuronal firing. In a study on awake and naturally sleeping cats, no sign of avalanches were found in neuronal firing (Bedard et al., 2006), and the apparent power-law scaling of LFP peaks could be explained as an artifact induced by the thresholding procedure used to detect LFP peaks. Previous studies have shown that even purely stochastic processes can display power-law scaling when subjected to similar thresholding procedures (Touboul and Destexhe, 2010). It was also stressed that power-law statistics can be generated by stochastic mechanisms other than SOC (Giesinger, 2001; Chialvo, 2010; Touboul and Destexhe, 2010).

These contrasting results correspond to different preparations and recording techniques, single units or LFPs, or different species, so that it is difficult to compare them. In the present paper, we attempt to overcome these shortcomings by providing a systematic analysis of both units and LFPs for different species and different brain states.

Materials and Methods

Recordings

Cat

Simultaneous recordings of multisite local field potentials (LFPs) and unit activity were obtained in the parietal cortex of awake cats, as published previously (Destexhe et al., 1999). A linear array of 8 bipolar electrodes (separated by 1 mm) was chronically implanted in the gray matter of area 5-7 of cat cerebral cortex. The state of the animal, as well as myographic and oculographic recordings, were

monitored to insure that brain states were correctly discriminated (quiet wakefulness with eyes-open, slow-wave sleep, REM sleep). LFP signals were digitized off-line at 250 Hz using the Igor software package (Wavemetrics, Oregon; A/D board from GW Instruments, Massachusetts; low pass filter of 100 Hz). Units were digitized off-line at 10 kHz, and spike sorting and discrimination was performed with the DataWave software package (DataWave Technologies, Colorado; filters were 300 Hz high-pass and 5 kHz low-pass).

Monkey

Recordings from three monkeys were used in this study. Each monkey was chronically implanted with 100-electrode Utah arrays (400 μ m inter-electrode separation, 1.0 mm electrode length; BlackRock Microsystems Inc., Salt Lake City UT). In two monkeys (A) and (B), we used recordings made during the performance of motor tasks. The motor tasks involved moving a cursor to visually-presented targets in the horizontal plane by flexing and extending the shoulder and elbow of the arm contralateral to the cerebral hemisphere that was implanted. In monkey (C), sleep recordings were used to test avalanche dynamics. Monkey A was implanted one array in primary motor cortex (MI) and a second array in dorsal premotor cortex (PMd) from which recordings were made on 64 electrodes in each cortical area. Monkey B had an array implanted in MI from which 96 electrodes were recorded. and Monkey C had two arrays in MI and PMd from which 96 electrodes were recorded in each area. During a recording session, local field potential (LFP) signals were amplified (gain, 5000), band-pass filtered (0.3 Hz to 250 Hz or 0.3 to 500 Hz), and recorded digitally (14-bit) at 1 kHz per channel. To acquire extracellular action potentials, signals were amplified (gain, 5000), band-pass filtered (250 Hz to 7.5 kHz) and sampled at 30 kHz per channel. For each channel, a threshold was set above the noise band: if the signal crossed the threshold, a 1.6ms duration of the signal - as to yield 48 samples given a sampling frequency of 30 kHz - was sampled around the occurrence of the threshold crossing and spike-sorted using Offline Sorter (Plexon, Inc., Dallas, TX).

Human

Recordings were obtained from two patients with medically intractable focal epilepsy using Neuroport electrode array as discussed previously (Peyrache et al., 2012, Truccolo et al., 2010). The NeuroPort electrode array, 1mm in length, was placed in layers II/III of the middle temporal gyrus in both patients. This array is silicon-based, made up of 96 microelectrodes with 400- μ m spacing, covering an area of 4 \times 4 mm. Since the corners are omitted from the array, the furthest separated contacts are 4.6 mm apart. Data were sampled at 30 kHz (Blackrock Microsystems, Salt Lake City, Utah, USA). The continuous recording was downsampled to 1250 Hz to obtain LFPs. The implantation site was included in the therapeutic resection in both patients. For details on spike sorting, see Peyrache et al. (2012).

Avalanche detection

Avalanches are defined by temporally contiguous clusters of activity among the different electrodes, separated by periods of silence. Either trains of neuronal action potentials (spikes) or or LFP peaks can occur in avalanches.

Spike avalanche

In each set of recordings, regardless of the spatial location of a given electrode in the multielectrode array, its spiking activity was put in the same pool with all other spikes recorded from other electrodes of the same array. This ensemble trace was then binned and coarse grained for different δt ranging from 1 ms to 16 ms in 2 ms steps. This created a series of bins containing the ensemble of activity across all neurons for that δt . The sum of spiking in that bin represents the total bin activity. The sum of all bin activities between two quiescent bins, represents the avalanche size, which was later used for statistical analyses.

Notice that in the case of the minimum $\delta t = 1$, avalanche size would range between 0 and maximum number of neurons present as this bin approximates the size unity of spiking period. Figure 1A shows the definition of avalanche in spike series from human recordings.

LFP avalanche

Each LFP trace was first detrended through a least-squares fit of a straight line to the data and subsequent subtraction of the resulting function from all the sample points. After this detrending removed the mean value or linear trend from a LFP vector, it was then normalized (Z score) to have a common reference frame for discretization across channels, recordings, states and species. The z-scored LFP, was then discretized through a local maxima peak detection. An optimizing small running average filter was designed and 3 passes of the filter were applied to the data in order to remove small spurious peaks in each LFP deflection. Next, by comparing each element of data to its neighboring values, if that sample of data was larger than both of its adjacent ones, that element was considered as a local peak. Next, all the peaks were sorted in descending order, beginning with the largest peak, and all identified peaks not separated by more than minimum peak distance (of 3 samples) from the next local peak were discarded.

The threshold was fixed and defined as a multiple of the standard deviation (STD) of the LFP signal. Different thresholds were tested, starting at $1.25 \times \text{STD}$ and increasing in 0.25 steps up to $5 \times \text{STD}$ for both negative and positive maxima. This procedure was realized on each LFP channel, state, species (Fig. 1B). Such matrix of discrete events (for a given polarity and a given threshold), was then treated the same way the spike matrix was used to create avalanche vectors of quiescent and active periods.

Testing power law distribution in empirical data

For testing the power-law behavior, usually a simple least square method is applied to fit a power-law on the data. If such fit in a log-log scale, follows a straight line, the slope of the probability density function (PDF) line is taken as the scaling exponent. Such method is widely practiced but is highly inaccurate in its estimation of true existence of power-law in a given dataset. It has been argued that, for obtaining statistically sound results in estimating power-law in empirical data, one has to rely on rigorous statistical methods. In a detailed analysis of the problem (Newman, 2005; Clauset et al., 2009), it was proposed that the cumulative distribution function (CDF) is much more accurate to fit the power-law exponent, as well as to identify if the system obeys a power-law.

If the initial distribution of the PDF is power-law, i.e.,

$$p(x) = Cx^{-\alpha} ,$$

then CDF is defined as

$$Pr(X > x) = C \int_x^{\infty} x'^{-\alpha} dx' = \frac{C}{\alpha - 1} x^{-(\alpha-1)} .$$

Thus, the corresponding CDF also behaves as a power-law, but with a smaller exponent

$$\alpha - 1$$

being 1 unit smaller than the original exponent (Newman, 2005).

Generally, in fitting the power-law to the empirical data, all the initial values (left hand of the distribution histogram i.e, smallest sizes of avalanches) are included in the used decades to obtain the slope of the fit (scaling exponent α). The inclusion of these initial parts may cause significant errors, and should be removed (Clauset et al., 2009; Bauke, 2007; Goldstein et al., 2004). Thus, before calculating the scaling exponent, it is essential to discard the values below the lower bound (X_{min}). It is only above this lower bound tha, a linear PDF or CDF can be reliably used for estimation of the scaling exponent. There are different methods for proper estimation of the X_{min} . We used a Kolmogorov-Smirnov (KS

test) optimization approach that searches for the minimum “distance” (D) between the power-law model and the empirical, where for $X_i \geq X_{min}$, “D” is defined as

$$D = \max |S(x) - P(x)| ,$$

$S(x)$ the CDF of the empirical data and $P(x)$ the CDF of the best matching power-law model. The X_{min} value that yields the minimum D, is the optimal X_{min} . The X_{min} is used in a maximum likelihood estimate (MLE) of power-law fit to the CDF of the avalanches in order to obtain the scaling exponent. This fitting, however, does not provide any statistical significance on whether the power-law is a plausible fit to the data or not. After the estimation of X_{min} and the exponent, we generated N (N=1000) power-law distributed surrogate data with the exact same features of X_{min} and exponent. Each of these surrogate series are then fitted with power-law and KS statistics of distance D (to the surrogate power-law), is performed. The fraction of N that the resultant statistics was bigger than the one obtained from the empirical data, comprises the p-value. If p-value ≥ 0.1 , the power-law is ruled out. However, even if p-value is larger than this threshold, the data is not necessarily guaranteed to be generated by a power-law process unless no better distribution is found to estimate the properties of the data. For this, the alternative test was adapted as following.

Generating power-law distributed random numbers with high precision

It is essential to use high precision and reliable algorithms to generate random numbers from a given probability distribution; otherwise the statistical tests based on such distributions may be erroneous. For initializing the generator with an “Integer Seed”, we adapted the reliable Mersenne Twister algorithm (known as MT19937AR) with full precision of Mersenne prime ($2^{19937} - 1$) (Mersenne et al., 1998). This algorithm provides a proper method for running Monte Carlo simulations. After initialization, “Transformation algorithm” was used to generate the desired distribution (Clauset et al, 2009, Press et al., 1992a). All the random number generations and analyses were performed on a 16-core Intel 48 GB Linux platform equipped with 448 core Tesla C2050 GPU with double precision of 515 Gflop and single precision of 1.03 Tflops. The custom code was based on Matlab (Mathworks) and CUDA (NVIDIA) wrapper Jacket (Accelreyes) for parallel computing on GPU.

Alternative fits

The power-law fit was compared with alternative hypotheses to test which distribution best fits the data. The alternatives included exponential distribution (as predicted by a Poisson type stochastic process), “Discretized log-normal distribution” (which is represented as a linear fit in log-normal scale), as well as fit of “Discrete exponential distribution” nature. These fits had two general types of simple exponential, defined as: $f(x) = a \exp(bx)$ as well as sum of exponential set as: $f(x) = a \exp(bx) + c \exp(dx)$ In each case, residual analyses, goodness of fit as well as confidence and prediction bounds were used to evaluate the properties of each fit vs power-law. In case of a good fit model, Residual, defined as the difference between data and fit, should approximate random error and behave randomly.

Goodness of fit comparison of exponential models

A measure of “goodness of fit”, R-square, is the ratio of the sum of squares of the regression (SSR) and the total sum of squares (SST). This measure, represents the square of the correlation between the observed and predicted response values, and indicates what percentage of the variance of the data is explained by the chosen fit (values of R-square range from 0, worst fit, to 1, the best possible fit). If we have SSR as: $SS_{reg} = \sum_i (\hat{y}_i - \bar{y})^2$, and SSE as: $SS_{err} = \sum_i (y_i - \hat{y})^2$, and SST as: $SS_{tot} = \sum_i (y_i - \bar{y})^2$, where, y_i, \bar{y}, \hat{y}

are the original data values, their mean and modeled values respectively. Then, it follows that:

$$R^2 = SS_{\text{reg}}/SS_{\text{tot}} = 1 - \frac{SS_{\text{err}}}{SS_{\text{tot}}}.$$

Correction by “total degree of freedom” and “error degree of freedom”, defines adjusted R-square:

$$\bar{R}^2 = 1 - (1 - R^2) \frac{N - 1}{N - M - 1} = 1 - \frac{SS_{\text{err}}}{SS_{\text{tot}}} \frac{df_t}{df_e}.$$

where “N” is the sample size, and “M” is the number of fitted coefficients (excluding constants). Usage of \bar{R}^2 in the comparison of “simple exponential” and “sum of exponential” is warranted by the fact that by an increase in the fitted number of the components, from one model to the other, the degrees of freedom changes. Both R^2 and \bar{R}^2 measures were estimated through nonlinear least square optimization of exponential curve fitting. In the optimization process for estimating the coefficients of the models, we adapted Levenberg-Marquardt algorithm with a tolerance of 10^{-8} (Press et al., 1992b).

Test of linearity in log-normal scale

Linearity in log-normal scale, is a hallmark of an exponential family process. In order to test the linearity of the PDF in log-normal scaling, we used Root mean square error (RMSE), $\text{RMSE}(\hat{\theta}) = \sqrt{\text{MSE}(\hat{\theta})}$ where MSE is: $\frac{SS_{\text{err}}}{df_e}$. This measure ranges from 0 to 1, where closer value to 0 is an indicator of a better fit.

This test was performed by fitting $y = \text{Log}(P(x))$ with a linear least square first degree polynomial. As shown in Fig. 12A, sometimes, the initial values in the left tail may slightly deviate from a simple 1st degree polynomial. Therefore, we tested whether the linearity was improved or worsened when the data range was reduced to above some X_{\min} . For doing so, we adapted a more stringent regression, bisquare robust 1st degree polynomial (Press et al., 1992b). This method is an iteratively reweighted least-squares, based on \bar{R}^2 , and assigns less weight to the values farther from the line. This procedure was repeated after excluding consequent single values from the left tail (up to 20 percent of the points). For each new shortened series, the RMSE (based on bisquare method) was re-calculated. The rational behind using RMSE for testing the linearity range in these datasets (with variable N) is that when a distinct point is removed from the dataset, 2 other reductions follow: a) the sum of squares and b) degrees of freedom. Thus, if after limiting the range, the error remains the same, SS_{err} would increase. Similarly, when the error is significantly reduced, SS_{err} would increase. Therefore, any change in the error, should only be considered significant if it is compensated by the amount of change in the degree of freedom. For quantifying this, we defined two measures for linearity improvement after limiting the data above X_{\min} . The first measure, “overall RMSE change” (oRMSE), was defined as:

$$oRMSE_i = \frac{RMSE_n - RMSE_{n-i}}{RMSE_n} * 100.$$

In parallel, “relative RMSE change” (rRMSE), was defined as:

$$rRMSE_i = \frac{RMSE_{n-i+1} - RMSE_{n-i}}{RMSE_n} * 100.$$

, where $RMSE_n$ was the RMSE of the full length data. Next, these measures were normalized to their maximum ($noRMSE$ and $nrRMSE$) and a 3rd dimension was created by the distance of each pair ($noRMSE_i$, $nrRMSE_i$), from the geometrical diagonal defined as

$$D = \frac{\det[(Q2 - Q1) \cdot (P - Q1)]}{\|(Q2 - Q1)\|}$$

, where P was the coordinates of a point ($noRMSE_i$, $nrRMSE_i$) while $Q1=[0\ 0]$ and $Q2=[1\ 1]$ were the vertices of the geometrical diagonal of the RMSEs pair space. The point that had the maximum “ $(1 - D_i) + noRMSE_i + nrRMSE_i$ ” (this value can range between 0 to 3), was taken as the optimal linearizing shortening index (X_{min}) (Fig. 12B). Next, we fitted all data ranges (from N sample points to $N - X_{min}$) with the two exponential models as described above.

Results

In this study, we used data from multielectrode recordings in 3 species: cat parietal cortex (8 bipolar electrodes), monkey motor cortex (three monkeys with a 64 or 96 recordings from 96 channel multielectrode arrays in motor and/or premotor cortex), and humans (2 patients with a 96 multielectrode array in middle temporal gyrus). In the following, we briefly address definition of avalanche, then describe the results of power-law analyses on spike avalanche, state-dependence, regional differences and polarity-dependence of LFP maxima avalanche. At the end, we briefly discuss alternative fits to the data.

Avalanche definition

Figure 1 illustrates the definition of avalanche for discrete (spike) and continuous (LFP) data, as they are used in this study. For both spikes and LFP, we used bins of 1 to 15 ms (in 2ms steps) for defining the quiescent vs active periods. Avalanches are defined by contiguous bins of non-zero activity, separated by periods of quiescence (empty bins). The size of the avalanche is defined as the sum of all activities (spikes or LFP peaks) within that avalanche. Thus, the avalanches depend on the bin size (as illustrated in Fig. 1A for spikes). For LFPs, we first discretized the continuous data based on its local maxima. Both positive and negative maxima were examined in our study. For each polarity, 17 levels of thresholds were chosen (see Methods for details). After discretization, the obtained matrix (Fig. 1B) was used for the same binning and avalanche definition as used for spike series.

Power-law fit

It has been shown that that CDF provides a a better measure than PDF as it avoids erroneous measures at the far end of the distribution tail of probability curve (Newman, 2005; Clauset et al., 2009). It is also necessary to exclude the values below the valid lower bound, or else the calculated coefficient could be highly biased (Clauset et al., 2009). In each of the following estimates of power-law distribution, based on the methods described previously, we adapted the following steps on analyzing the CDF of avalanches: Values above a given X_{min} are used in a maximum likelihood estimate (MLE) of the exponent α . For each CDF, the proper lower bound of X_{min} is selected using a KS test. We also used 1000 semi-parametric repetitions of the fitting procedure for obtaining estimates of uncertainty and goodness of fit.

Avalanche analysis from spikes

Next, we studied whether the spike avalanches follow power-law distributions.

Avalanche analysis in wakefulness

We first studied avalanche dynamics in awake resting recordings from cats and humans. As depicted in Fig. 2, neither of these species, showed a dominant power-law behavior in their spike avalanche size distribution. The average scaling exponent of awake recordings for the decades that could be considered to follow power-law (i.e. $>X_{min}$), was too high to be related to SOC systems (see Table. 1 and Table. 2 and Fig. 2.i,ii,iii). These values not only are distant from those of 1/f noise, but also only apply to partial parts of the CDF (cumulative distribution function) of avalanche sizes. These lack of clear power-law

characteristics is shown with X_{min} lower boundary (green dotted lines in Fig. 2). Only values above X_{min} could "statistically" follow a power-law regime and as mentioned, even in those cases, the exponent values were too high to be considered a signature of SOC systems.

Interestingly, representing the size distributions in log-linear scale revealed a scaling very close to linear for all species (Fig. 3), indicating that avalanches defined from spikes scale close to an exponential, as would be predicted by a Poisson-type stochastic process. This conclusion was also reached previously by analyzing units and LFP recordings in cats (Bedard et al., 2006).

In addition to wake resting recordings, we also considered recordings made while monkeys engaged in cognitive motor tasks. Similar to awake resting recordings in cat and man, the lower bound was variable between different binning sizes, thus excluding parts of the "invalid" initial avalanche sizes, which are usually used as evidence of existence of power-law (Beggs and Plenz, 2003; Petermann et al., 2009; Klaus et al., 2011). The inclusion of these initial parts may cause errors, and were removed here (Newman, 2005; Clauset et al., 2009; Bauke, 2007; Goldstein et al., 2004). Above the lower bound value, all the CDF curves showed significant high exponent values. Interestingly, the MI (in both monkeys A and B) had similar mean to PMd (Table. 1, Fig. 2D,E,F), suggesting similar dynamics in the two areas.

Avalanche analysis during natural sleep

It has been claimed that wakefulness may not be the best state to display SOC, and that avalanches may be more naturally related to brain states with oscillations, and slow-wave oscillations in particular (Hahn et al., 2011). In contrast to this, a previous study in cat found that like wakefulness, slow-wave sleep (SWS) did not display power-law scaling as defined from spike avalanches (Bedard et al., 2006), but this latter study suffered from a limited spatial sampling. To further investigate the issue, we have examined SWS and Rapid Eye Movement (REM) sleep periods with more dense sampling of spike activity. Figures 4 and 5, show the analyses for cat, human A and B as well as monkey C (MI and PMd) for SWS and REM periods. In none of these cases we see clear sign of power-law scaling. In all cases (except human B), the variability of lower bound between different bin sizes is robust. All the curves represent "partiality of power-law" with high exponent values. During SWS, cat, human subjects and monkey C (MI and PMd) all manifested either lack of significant power-law scaling, or had such higher exponent values that makes it highly unlikely for power-law to be the generating process of spike dynamics (Table. 1). Similarly, in REM periods, there was no evidence for power-law scaling in human A's first and second REM episodes. Together, with Cat REMs' high exponents values, power-law scaling appears to be an unlikely candidate to describe the statistics of neural firing (Table. 1). Taken together, these various tests all based on proper statistical inferences, show that spike avalanches do not follow power-law scaling, for any brain state or sampling density.

Detailed numerical values for spike avalanche CDF exponents and their goodness of fit are provided in Table. 1 and Table. 2.

Avalanche dynamics from local field potentials

Next, we investigated the occurrence of avalanche type of dynamics from the local field potentials, which were simultaneously recorded with unit activity, in all datasets.

Relation between LFP peaks and spiking activity

Calculation of neuronal avalanches from LFP data is based on the assumption that the negative LFP (nLFP) peaks are related to neuronal activity (e.g., see Petermann et al., 2009). Indeed, the cat LFP data analyzed here was show to display such a relation (Destexhe et al., 1999; Touboul and Destexhe, 2010). To further test this relation, we also examined the simultaneous LFP and unit recordings in man and monkey. We used a wave-triggered-average (WTA) procedure, where the ensemble of nLFPs were

used to epoch the ensemble spike activity. Averaging across these WTAs across different thresholds, show that there is indeed a weak relationship between nLFP and spiking (Fig. 6A). However, repeating the same procedure for positive LFP (LFP) peaks, did not display any relation (Fig. 6B), in agreement with the same analysis in cats (Touboul and Destexhe, 2010). This fundamental difference between nLFP and pLFP peaks provides a very important test to infer if a given power-law observation from LFPs is related to the underlying neuronal activity, as we will see below.

nLFP avalanches

Similar to previous studies, we investigated the avalanche dynamics from nLFPs. The nLFPs were detected using a fixed threshold, defined as a multiple of the standard deviation (STD) of the LFP signal (see Methods), and several thresholds were tested. In the following, we use “high”, “medium” and “low” thresholds, which correspond to 2.25, 1.75 and 1.25 multiples of the standard deviation, respectively. As shown in Figs. 7 and 8, the distributions defined for avalanches at different bin sizes and thresholds seem to display power-law scaling, both for human and monkey. This result seems to be in agreement with similar analyses done on awake monkey (Petermann et al., 2009). However, plotting the same data as CDF revealed that the scaling as power-law was very narrow (Fig. 9). While Monkey B displayed apparent power-law over more than one decade, the other cases from cats and humans, did not display any convincing power-law scaling. For details of nLFP avalanches for an example subject, and its comparison with pLFP avalanches, see Table. 3.

pLFP avalanches

Next, we investigated the avalanche dynamics of positive LFP peaks, which, as we have seen above, is not statistically related to firing activity (Fig. 6). Similar to nLFP peaks, the pLFP avalanches defined for human wakefulness did not display power-law scaling (Fig. 10). Both nLFP and pLFP had similar CDF of avalanche size across different species and cortices. The example shown in Fig. 10 (awake human) shows that across different thresholds, both nLFP and pLFP had variable lower bounds and high scaling exponents for the region of the data that could statistically be considered for power-law properties. Moreover, the absence of any region with clear linear scaling in the logarithmic coordinates further confirms that there is no power-law scaling in this case. For details, see Table. 3.

Avalanches in different cortical regions

In the cases that we had simultaneous, dual array multielectrode recordings from PMd and MI, the analyses showed that these two cortical areas do not show signs of criticality but have slight differences in their exponent values for MI and for PMd (Table. 1 and Table. 2, Fig. 11). Such findings show that the fact that these two cortices directly interact with each other, and one acts as input and one as the output of motor processing unit, is reflected in their slightly different CDF features. Thus, two different cortical areas seem to display similar features, although no sign of power-law scaling.

Statistical analysis of the avalanche distributions

Goodness of fit

Given data x and given lower cutoff for the power-law behavior X_{min} , we computed the corresponding p-value for the Kolmogorov-Smirnov test, according to the method described in Clauset et al. (2009). See methods for details. The results are given in Tables 1, 2 and 3 (“gof” columns).

Alternative distributions for avalanche dynamics

Although previously, at the microcircuit scale, some studies have asserted the existence of criticality as a universal characteristic of neural dynamics in both spike and LFP avalanches (Beggs and Plenz, 2003; Ribeiro et al., 2010), other evidence suggest that same behavior can also be observed through stochastic processes (Bedard et al., 2006; Touboul and Destexhe, 2010). In this study, after rigorous testing, we showed that the avalanches do not follow power-law as a universal feature. Thus we also tested whether an alternative probability distribution could provide a better estimate for the experimental observations.

We first tested a simple exponential fitting of the spike avalanches, by fitting straight lines in a log-linear plot. As seen from Fig. 12A, a linear fit (“exp1”) can only fit part of the data, as the initial points (for small size) do not scale linearly. In detection of the lower bound of linearity, i.e. (X_{min}), the robust bisquare method is more stringent than simple least square fits and leaves behind more datapoints for exponential fitting (see different lines in Fig. 12A; errors based on bisquare are plotted in Fig. 12B; see Methods for details on linearity optimization).

Next, we tested a multiple exponential fitting of the data. The rationale is that two exponential processes may represent differences in two populations of cells, for example excitatory and inhibitory cells. The fit resulting from a “sum of exponential processes” was extremely good in minimum residual and reliable prediction bounds for the data (Fig. 12C). This “sum of exponential” model (“exp2”) gave a very good performance in both full length (dark blue) and reduced above “ X_{min} ” (red). The “simple exponential” model (exp1) reaches a very good fit only for the reduced set (cyan) but not for the full length of the avalanches (light brown). For comparison of “exp1” and “exp2” on different spike avalanches, with and without “linearity improvement”, see Fig. 12D. Overall, it seems that both exp1 and exp2 exhibit comparably high values of goodness of fit for the reduced sets. However, only the double exponential fit was able to fit the entire dataset.

Discussion

In the present paper, we have analyzed and compared the avalanche dynamics obtained from multielectrode recordings of spikes and LFPs, for three species, cat, monkey and human. In each case, we used recordings exclusively made in non-anesthetized brain states, including quiet and active wakefulness, SWS (slow-wave sleep) and REM (Rapid eye movement). The primary result of our analysis is that there is no power-law scaling of neuronal firing, in any of the recordings, including “desynchronized” EEG states (wakefulness), SWS, and REM sleep. All species consistently showed distributions which approached exponential distributions. This confirms previous findings of the absence of power-law distributions from spikes in cats (Bedard et al., 2006), and extends these findings to monkeys and humans.

In contrast, avalanche dynamics built from nLFPs displayed more nuanced results. In some cases, the avalanche size distributions appear to draw a straight line in log-log representations, but the more reliable CDF-based tests did not show clear evidence for power-law scaling. Indeed, statistical tests such as the KS test did not give convincing evidence that these data are universally distributed according to a power-law. More importantly, while nLFP are related to firing activity, we showed that a similar behavior was also observed for pLFP peaks. The avalanche analysis from positive peaks displayed similar results as for negative peaks, although positive peaks are not related to firing activity. Together, these results suggest that the power-law behavior observed previously in awake monkey (Petermann et al., 2009, Ribeiro 2010) cannot be reproduced in awake humans’ temporal cortex or monkey motor cortex. This conclusion also extends to slow-wave sleep and REM sleep, which we found did not display power-law distributed avalanches, as defined from either spikes or LFPs.

A possibility worth exploring is that some form of power-law in LFPs is the result of volume conduction associated with LFPs recorded in high density arrays. When a peak is detected, it is often also present in many different channels. A possibility worth to explore is whether the same event could be volume-

conducted across many channels in the array, which may lead to an artificial increase the large-size avalanches. This possibility should be examined by mathematical models of the volume conduction effect.

It must be noted the evidence for self-organized criticality in neuronal cultures or in slices (Beggs and Plenz, 2003), as well as in anesthetized states (Hahn et al., 2010) is not contradictory with the present findings. The wiring of *in vitro* preparations, as well as the network dynamics in anesthesia, are evidently different than in the intact brain. We find here that there is no evidence for SOC in wakefulness and natural sleep states, and for 3 different species. On the other hand, the report of power-law scaling of nLFPs avalanches in awake monkey (Petermann et al., 2009) seems in contradiction with the present findings. Many possibilities exist to reconcile these observations, such as differences between brain region, recording method, cortical layer or volume conduction effects. These possibilities should be investigated in future studies.

Finally, it is important to emphasize that the present results were obtained using stringent statistical tests, similar to previous statistical analyses (Newman, 2005; Clauset et al., 2009). The use of the CDF distribution rather than simple log-log representations of the size distribution is a particularly severe test to identify if a system scales as a power-law. The use of statistical measures such as the Kolmogorov-Smirnov test (Table. 1, 2 and 3) also constitutes a good quantification of which distribution fits the data, and is largely superior to the least square fit in double logarithmic scale (Clauset et al., 2009). The uncertainty and goodness of fit were estimated by 1000 repetitions of each fitted distributions. Taken together, these tests represent an unprecedented level of quantification and analysis, which we believe is a useful step towards understanding the type of dynamics exhibited by the awake and sleeping brain.

Acknowledgments

Research supported by Centre National de la Recherche Scientifique (CNRS, France), Agence Nationale de la Recherche (ANR, France), European Community Future and Emerging Technologies program (BRAIN-SCALES grant FP7-269921) and the National Institutes of Health (NIH grants 5R01NS062092, R01 EB009282). N.D. is supported by a fellowship from Ecole de Neurosciences de Paris (ENP).

References

- Bak 1987, Bak, P., Tang, C. , Wiesenfeld, K. Self-organized criticality: An explanation of the $1=f$ noise. Phys. Rev. Lett. 59, 381-384 (1987).
- Bak 1995, Bak P, Paczuski M. Complexity, contingency, and criticality. PNAS 1995.
- Bak 1996, P. Bak, How Nature Works (Springer-Verlag, New York, 1996).
- Bauke 2007, H. Bauke, Parameter estimation for power-law tail distributions by maximum likelihood methods, Eur. Phys. J. B, 58 (2007), pp. 167173.
- Bedard 2006, Bedard, C., Kroger, H., , Destexhe, A. (2006). Does the $1/f$ frequency-scaling of brain signals reflect self-organized critical states? Physical Review Letters, 97, 118102.
- Bedard 2006b, Bedard, C., Kroger, H., , Destexhe, A. (2006). Model of low-pass filtering of local field potential in brain tissue. Phys Rev E Stat Nonlin Soft Matter Phys, 73:051911.
- Begs 2003, Beggs JM, Plenz D (2003) Neuronal avalanches in neocortical circuits. J Neurosci 23:1116711177
- Chialvo 2010, Chialvo D, Emergent complex neural dynamics, Nature Physics, 2010.
- Clauset 2009, A. Clauset, C.R. Shalizi, and M.E.J. Newman, "Power-law distributions in empirical data" SIAM Review 51(4), 661-703 (2009)
- Frette 1996. Avalanche dynamics in a pile of rice. Nature. 1996
- Giesinger 2001 Giesinger, T. Scale invariance in biology: coincidence or footprint of a universal mechanism? Biol. Rev. 76, 161-209 (2001).

- Goldstein 2004, M. L. Goldstein, S. A. Morris, and G. G. Yen, Problems with fitting to the power-law distribution, *Eur. Phys. J. B*, 41 (2004), pp. 255258.
- Hahn 2010, Hahn G, Petermann T, Havenith MN, Yu S, Singer W, et al. (2010) Neuronal avalanches in spontaneous activity in vivo. *J Neurophysiol*.
- Hahn 2011, Hahn G, Monier C and Frégnac Y. Revisiting power law in vivo as a function of the global brain state, using multiple recordings in anesthetized cat V1. *Soc. Neurosci. Abstracts* 451.10, 2011.
- Jensen 1998, H. J. Jensen, Self-Organized Criticality: Emergent Complex Behavior in Physical and Biological Systems (Cambridge University Press, Cambridge, England, 1998).
- Klaus 2011. Klaus A, Yu S, Plenz D (2011) Statistical Analyses Support Power Law Distributions Found in Neuronal Avalanches. *PLoS ONE* 6(5): e19779
- Malamud 1988, Malamud, B. D., Morein, G., Turcotte, D. L. Forest fires: An example of self-organized critical behaviour. *Science* 281, 1840-1842 (1998).
- Mersenne 1998 Matsumoto, M.; Nishimura, T. (1998). "Mersenne twister: a 623-dimensionally equidistributed uniform pseudo-random number generator". *ACM Transactions on Modeling and Computer Simulation* 8 (1): 330.
- Newman 2005. Newman, Power laws, Pareto distributions and Zipf's law *Contemporary Physics* 46, 323-351 (2005)
- Petermann 2009 Petermann, T. Thiagarajan TC, Lebedev MA, Nicolelis MA, Chialvo DR, et al. Spontaneous cortical activity in awake monkeys composed of neuronal avalanches. *Proc. Natl Acad. Sci. USA* 106, 15921-15926 (2009).
- Peters 2006, Peters, O., Neelin, D. Critical phenomena in atmospheric precipitation. *Nature Phys.* 2, 393-396 (2006).
- Peyrache 2012, Adrien Peyrache, Nima Dehghani, Emad Eskandar, Joseph Madsen, William Anderson, Jacob Donoghue, Leigh R Hochberg, Eric Halgren, Sydney S. Cash and Alain Destexhe, Spatio-temporal dynamics of neocortical excitation and inhibition during human sleep., *PNAS* : , (2012)
- Press 1992a Press, W. H.; Flannery, B. P.; Teukolsky, S. A.; and Vetterling, W.T. "Random Numbers." Ch. 7 in *Numerical Recipes: The Art of Scientific Computing*, 3rd ed. Cambridge, England: Cambridge University Press, pp. 266-306, 1992.
- Press 1992b Press, W. H.; Flannery, B. P.; Teukolsky, S. A.; and Vetterling, W.T. "Nonlinear models." Ch. 15 in *Numerical Recipes: The Art of Scientific Computing*, 3rd ed. Cambridge, England: Cambridge University Press, pp. 266-306, 1992.
- Ribiero 2010, Ribeiro T, Copelli M, Caixeta F, Belchior H, Chialvo DR, Nicolelis M, Ribeiro S. Spike Avalanches Exhibit Universal Dynamics across the Sleep-Wake Cycle. *Plos One* 2010.
- Steriade 2001. Steriade M. The intact and sliced brain.
- Toboul 2010 Toboul, J., Destexhe, A. Can power-law scaling and neuronal avalanches arise from stochastic dynamics? *PLoS One* 5, (2010).
- Truccolo 2010 Truccolo, W., Hochberg, L., Donoghue, J. (2010). Collective dynamics in human and monkey sensorimotor cortex: Predicting single neuron spikes. *Nature Neuroscience*, 13, 105111.

Figures

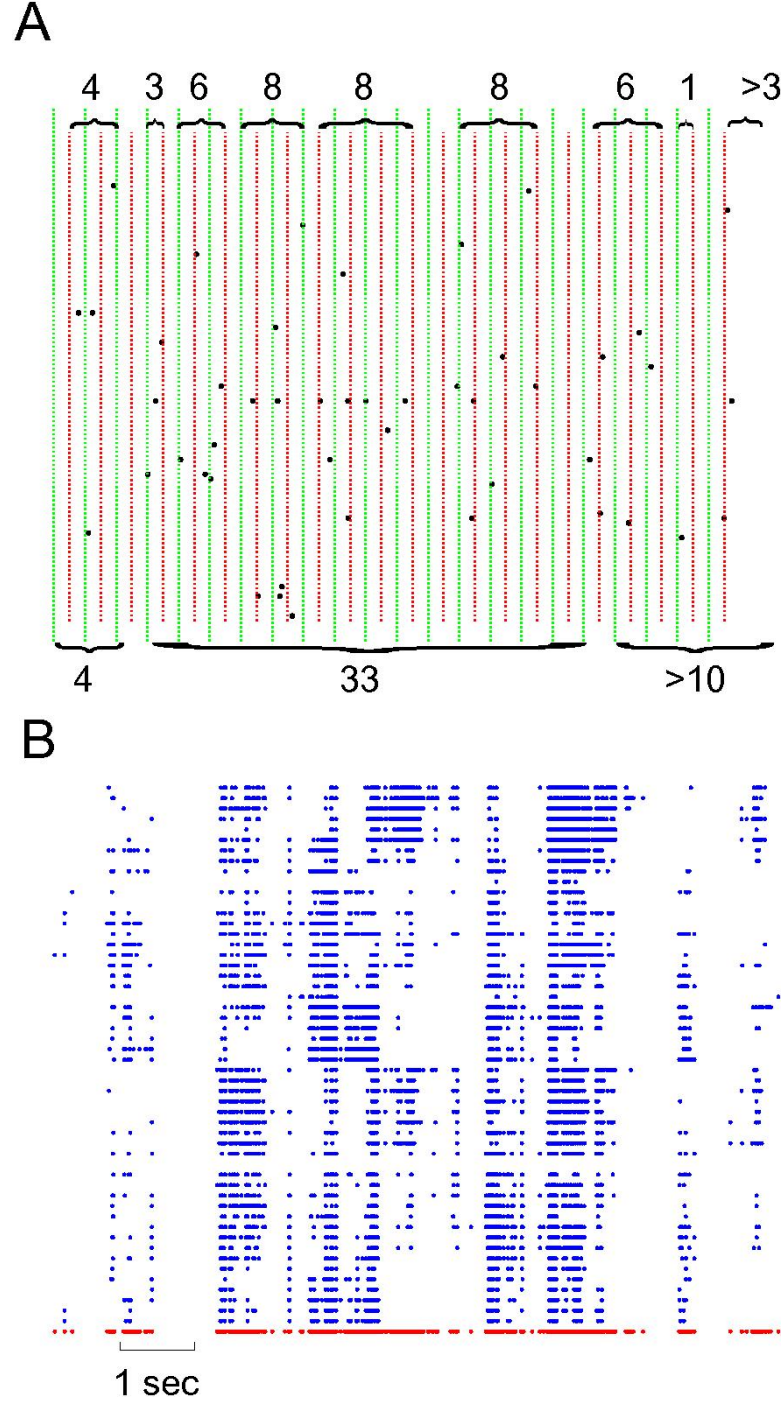


Figure 1. Definition of avalanches. i) comparison of avalanche definition for 8ms vs 16 ms binning; green vertical lines define the boundaries of 16ms binning; naturally, each 16ms bin is composed of 2 independent 8ms bin (depicted with red dotted lines). Accolades point to the avalanches, separated by quiescent periods. Top, 8ms avalanches and their sizes, Bottom: 16ms avalanches and their corresponding size. Please note that last avalanche continues after of the limits in this figure. ii) negative local maxima obtained from the grid of electrodes for a period of 10 sec. Each row represents negative maxima of a single LFP channel of a selected threshold level $\geq 1.75 \times \text{STD}$ of the normalized LFP. The red dots in the bottom refer to ensemble presence of nLFP maxima.

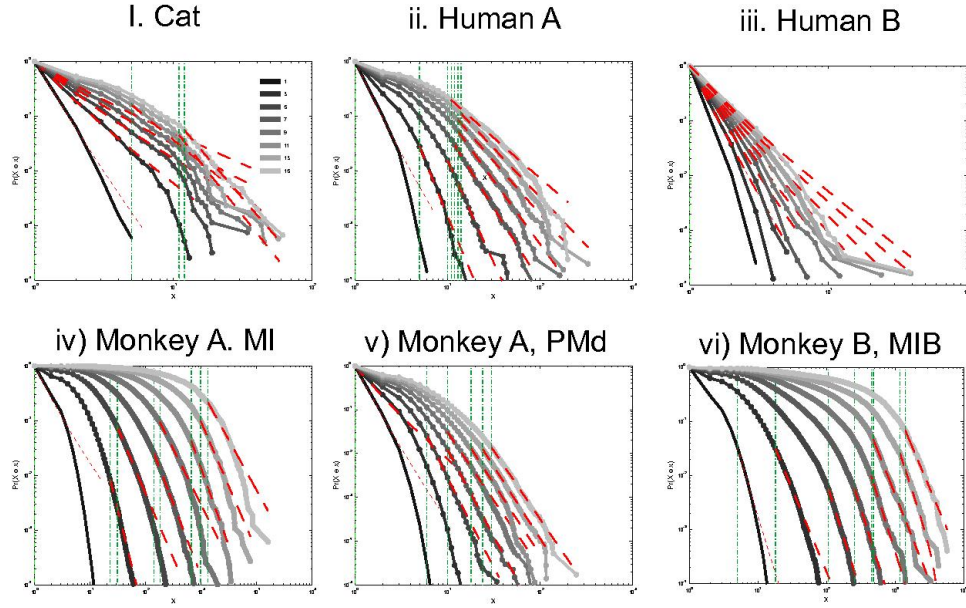


Figure 2. Avalanche analysis on spiking activity during wakefulness. In idle awake ,i). Cat, ii). Human A, iii). Human B. Different line colors refer to different bin sizes as shown in the legend. The lower bound (X_{min} , shown in green dotted line), shows that the CDF of avalanche size, only partially, may follow power-law distribution. Even in such cases, the exponents had very high values, well above the criticality regime that is hypothesized for $1/f$ noise. Panels iv,v and vi, show the same type of curves for monkeys engaged in cognitive motor task. Same pattern is observed; it also seems MI has slightly higher values than PMd in the plausible power-law regime. For the mean/std exponent values, see Table. 1 and Table. 2.

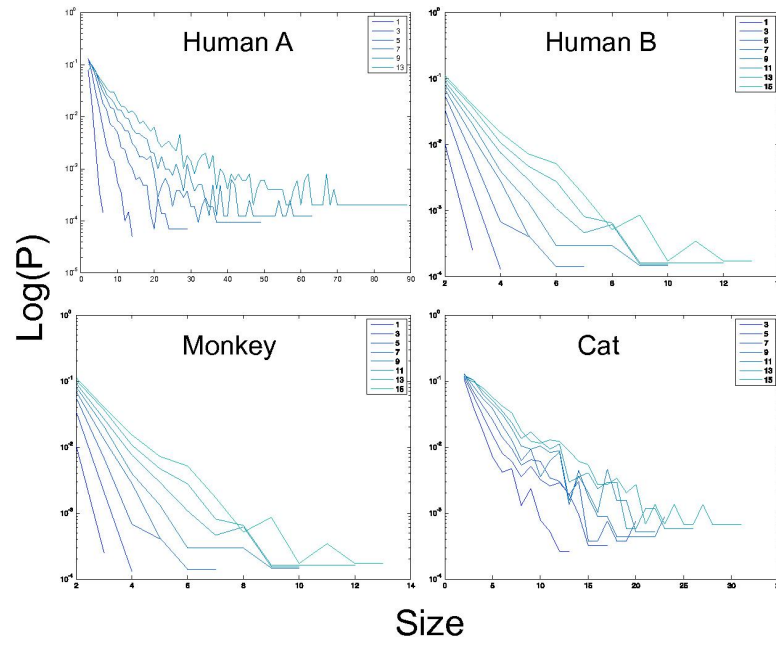


Figure 3. Spike avalanche distributions in log-linear representation. Different line colors refer to different bin sizes as shown in the legend. An exponential process has a linear trend in log-linear scale. Spike avalanches for all coarse graining levels, showed a linear trend. Please notice that bin sizes 11 and 15 are not shown because for the clarity in the line plot, but showed similar linear trend in this scale (not shown).

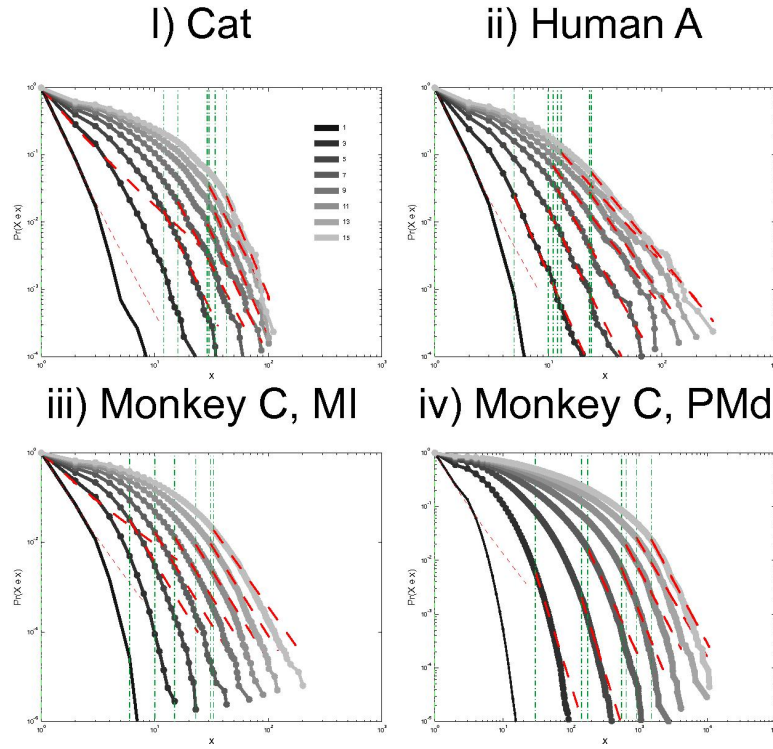


Figure 4. Avalanche analysis of spiking activity during slow-wave sleep. i) Cat, ii) Human A, iii) human B, iv) monkey C MI and v) monkey C PMd. Different line colors refer to different bin sizes as shown in the legend. In parallel to awake dynamics (Figure 2), there is no sign of criticality, the curves follow different partial power-law with high exponents and variable lower bound values. The avalanche dynamics do not show a state-dependent trend. For the mean/std exponent values, see Table. 1.

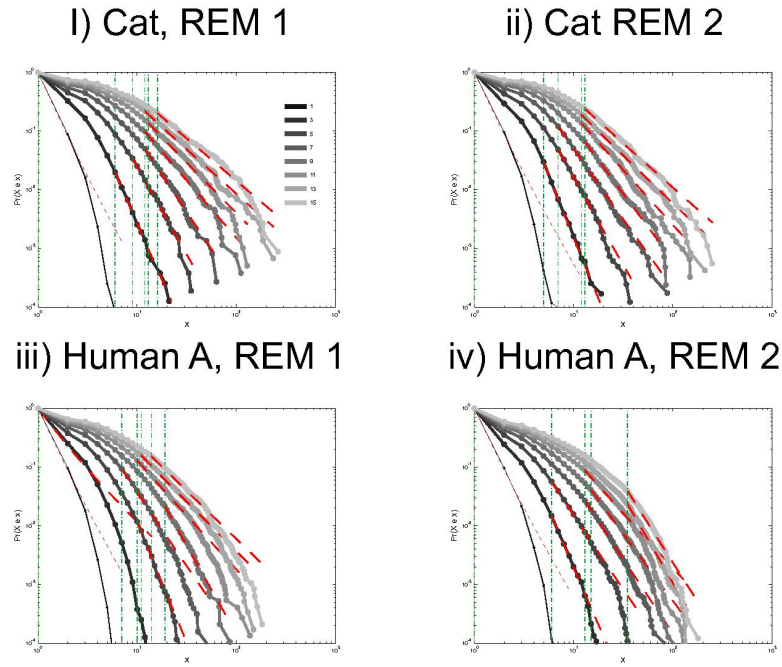
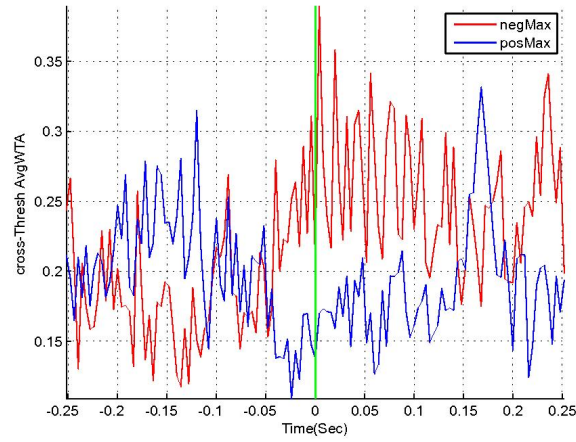


Figure 5. Avalanche analysis of spiking activity during REM sleep. i) cat REM episode 1, ii) cat REM episode 2, iii) human A REM episode 1, iv) human A REM episode 2. Different line colors refer to different bin sizes as shown in the legend. Similar to awake and SWS, the lack of criticality, variability through different coarse graining thresholds and lower bounds is the universal finding. For the mean/std exponent values, see Table. 1.

A. Cat ensemble WTA



B. Human A ensemble WTA

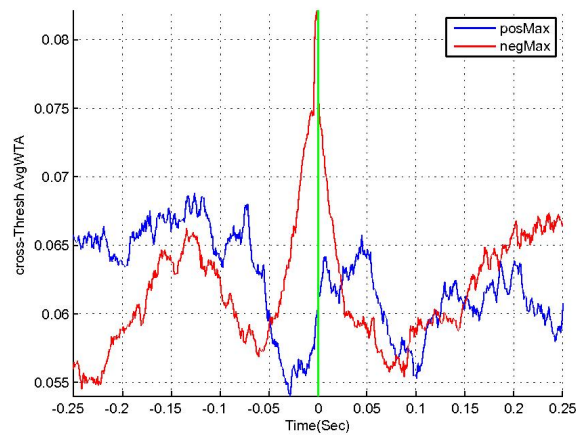


Figure 6. Relation between unit firing and LFP peaks in wakefulness. nLFP (red) and pLFP(blue)-based wave-triggered average (WTA) of unit activity, showing that the negative peaks have slightly higher association with an increase of neuronal firing.

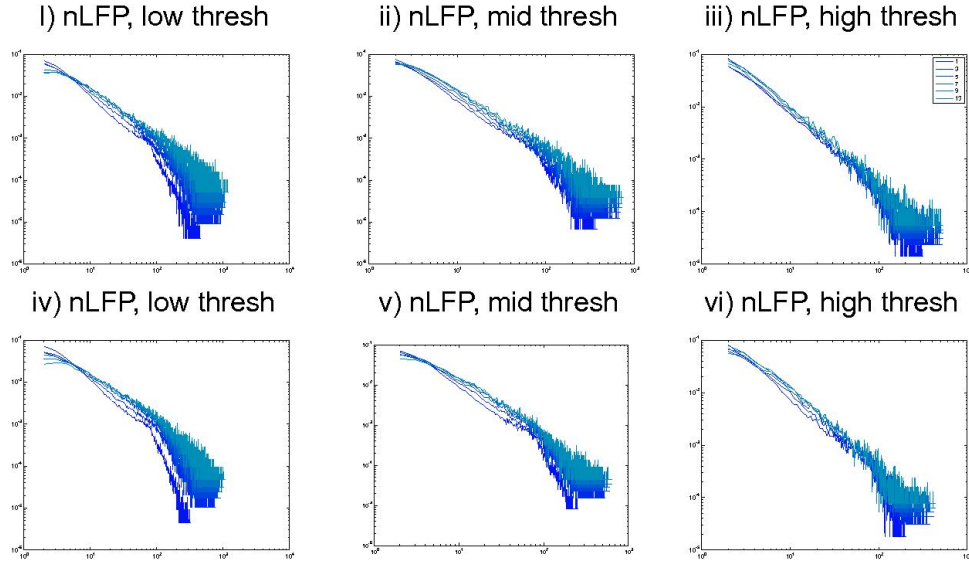


Figure 7. Avalanche analysis in awake monkey LFPs in logarithmic representation. A power-law process has a linear trend in log-log scale. LFP (negative or positive) maxima avalanches for all coarse graining levels, as well as all thresholds, showed a linear trend. Please notice that bin sizes 11 and 15 are not shown because for the clarity in the line plot; however, they too, also showed a very clear linear trend in this scale. Such trend is necessary but not sufficient for a process to be power-law. See text and Fig. 9

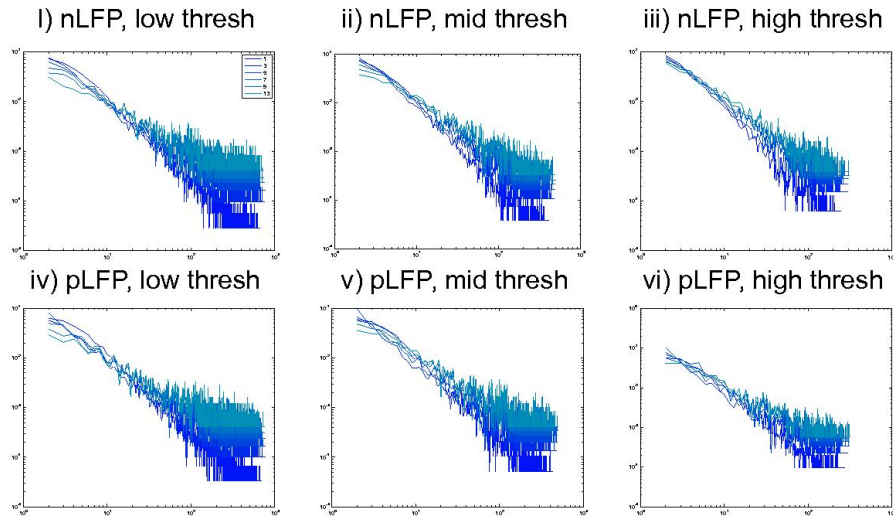


Figure 8. Avalanche analysis in awake human LFP in logarithmic representation. A power-law process has a linear trend in log-log scale. LFP (negative or positive) maxima avalanches for all coarse graining levels, as well as all thresholds, showed a linear trend. Please notice that bin sizes 11 and 15 are not shown because for the clarity in the line plot; however, they too, also showed a very clear linear trend in this scale. Such trend is necessary but not sufficient for a process to be power-law. See text and Fig. 9

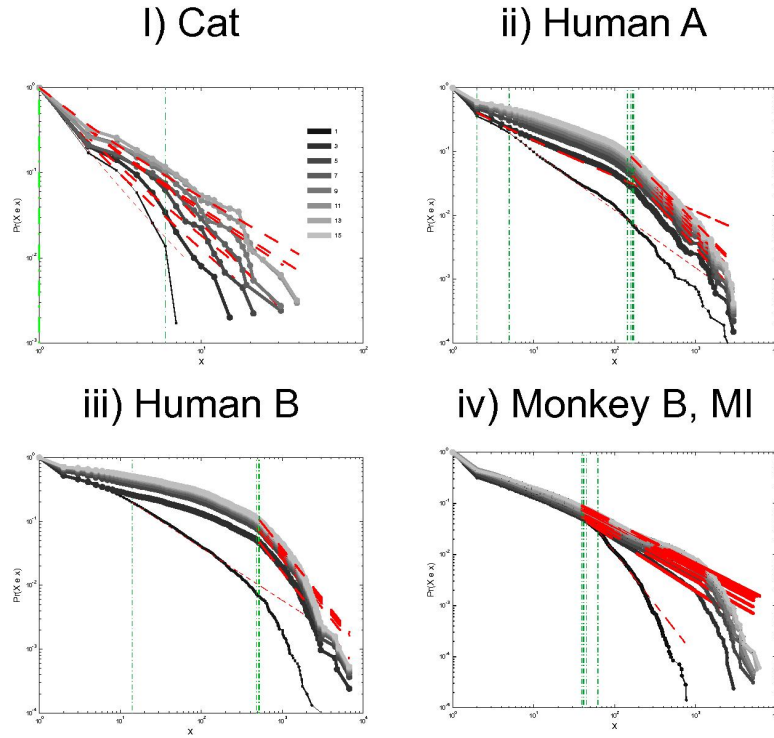


Figure 9. Avalanche analysis based on LFP negative peaks in wakefulness. i) Cat, ii) Human A, iii) Human B, iv) Monkey B MI. In all cases, different binnings lead to variable lower bound and scaling exponents. Lack of linear trend in CDF shows that the observed linear trend in log-log scale, as shown in Fig. 7 and Fig. 8, are not sufficient for showing that avalanche dynamics are power-law processes. For the mean/std exponent values, see Table. 3.

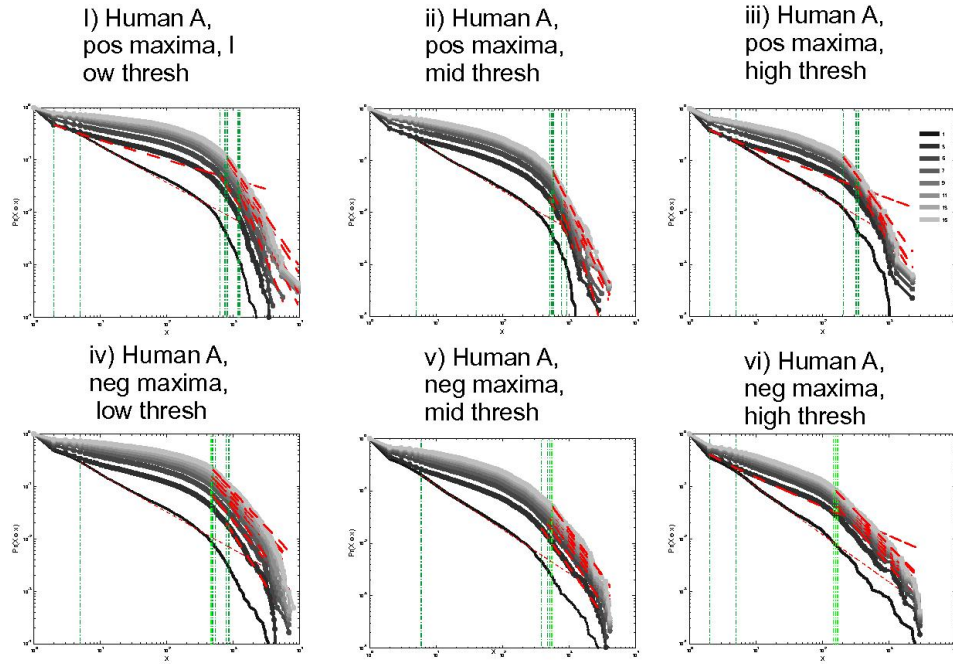


Figure 10. Comparison of Avalanche analysis based on negative and positive peaks. LFP (negative or positive) maxima avalanches for all coarse graining levels, as well as all thresholds did not show linear trend in CDF, therefore negate power-law as the generating process. These curves show while nLFP has a closer relation with spiking, the avalanche dynamics of nLFP and pLFP are strikingly similar in their lack of robust criticality when tested with rigorous statistical tests.

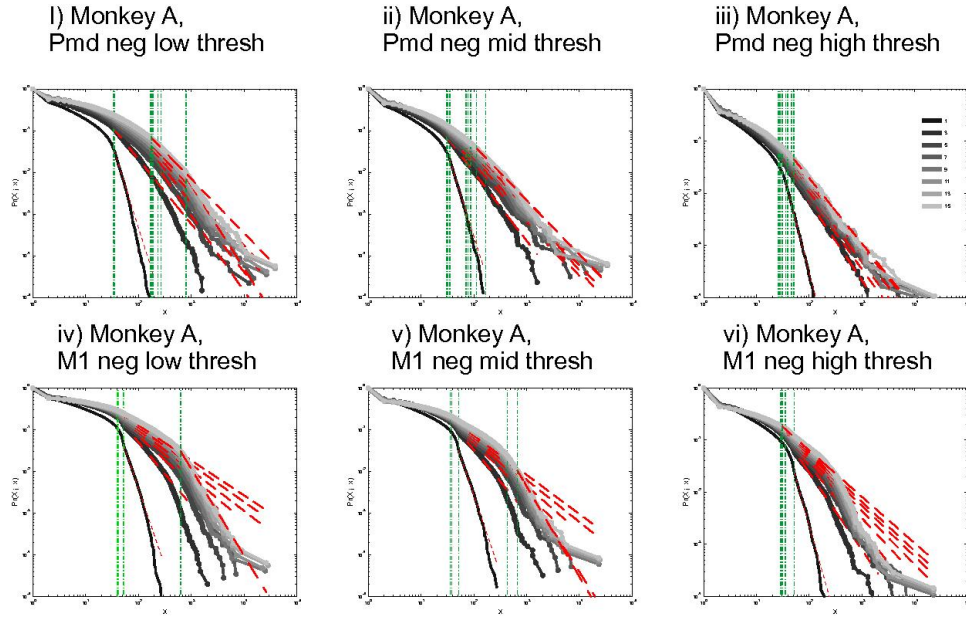


Figure 11. Avalanche analysis in different cortical areas recorded simultaneously.

Avalanche dynamics in nLFP shows that the CDF of the input and output units of two interacting cortices have slightly different characteristics but neither follow criticality regime. i)Monkey A, MI, low threshold ii)Monkey A, MI, medium threshold, iii)Monkey A, MI, high threshold, iv)Monkey A, PMd, low threshold v)Monkey A, PMd, medium threshold, vi)Monkey A, PMd, high threshold.

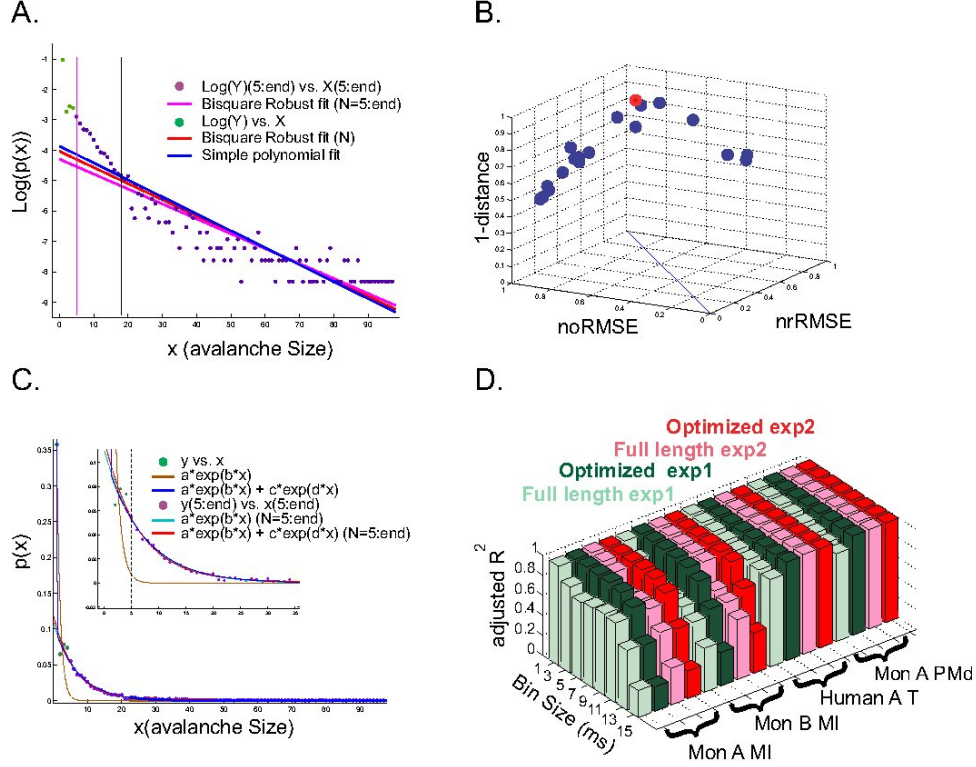


Figure 12. Alternative fits for avalanche size distributions. A. Simple exponential fitting of spike avalanche data. The datapoints (purple and green) are plotted in a log-linear representation, together with a simple polynomial fit (blue), a robust fit calculated on the full length data (red) and a robust fit on the reduced data (magenta). The two vertical lines indicate the lower bound of the region of linearity, i.e. " X_{\min} ", calculated based on the simple polynomial fit (black) and the bisquare method (magenta). B. Comparison of the goodness of fit of different exponential fits to different reductions of the same dataset. The 3 coordinates are "normalized overall improvement of RMSE" (noRMSE), "normalized relative improvement of RMSE" (nrRMSE) and distance of a point from the diagonal in (noRMSE, nrRMSE) plane. Each point in this 3D space, is the result of a bisquare robust fit after elimination of the first i elements of the data (best fit in red). C. Bi-exponential fitting of the same data. The "sum of exponential" model (exp2) gave a very good performance in both full length (dark blue) and reduced above " X_{\min} " (red). The "simple exponential" model (exp1) reaches a very good fit only for the reduced set (cyan) but not for the full length of the avalanches (light brown). D. Effects of linearity improvement on exponential fits. Each set of four colours refer to the spike avalanche of Monkey A(MI), Monkey B(MI), Human A(Temporal) and Monkey A(PMd). In each set, green colors refer to the simple exponential family (exp1) and the red colors depict the sum of exponentials (exp2). Light green and light red, refer to the calculated \bar{R}^2 on full length avalanche sizes, while dark green and dark red show the average \bar{R}^2 for the dataset ranging from $N - 1$ to $N - X_{\min}$ where the optimized length X_{\min} was 5 (see panels B and C). Panels A, B and C were obtained from 15 ms bin avalanches from human A awake spikes.

Tables

Table 1. Summary spike avalanche

<i>Species</i>	<i>Loc</i>	<i>State</i>	<i>CDF exponent</i>	<i>Pval</i>	<i>gof</i>
Monkey A	MI	Awake	3.4413 ± 0.7616	0.0419 ± 0.1152	0.0442 ± 0.0216
Monkey A	Pmd	Awake	4.1660 ± 0.6590	0.1130 ± 0.2140	0.0180 ± 0.0050
Monkey B	MI	Awake	4.6250 ± 0.4730	0.4550 ± 0.3600	0.0330 ± 0.0120
Monkey C	MI	SWS	4.5560 ± 0.7980	0.0030 ± 0.0100	0.0220 ± 0.0080
Monkey C	Pmd	SWS	3.7760 ± 0.8660	0 ± 0	0.0430 ± 0.0170
Cat	Parietal	Awake	3.1410 ± 0.8720	0.2010 ± 0.3680	0.0270 ± 0.0180
Cat	Parietal	SWS	4.2110 ± 0.7930	0.3290 ± 0.3620	0.0350 ± 0.0140
Cat	Parietal	REM 1	3.3240 ± 0.8150	0.2990 ± 0.2170	0.0290 ± 0.0110
Cat	Parietal	REM 2	3.4050 ± 0.8250	0.4250 ± 0.4470	0.0230 ± 0.0140
Human A	Temporal	Awake	3.5490 ± 0.8790	0.3870 ± 0.3650	0.0210 ± 0.0080
Human A	Temporal	SWS 1	3.6340 ± 0.6410	0.3790 ± 0.3150	0.0250 ± 0.0100
Human A	Temporal	SWS 2	3.2550 ± 0.5770	0.1710 ± 0.2670	0.0330 ± 0.0150
Human A	Temporal	REM 1	3.3740 ± 0.8560	0.0930 ± 0.1720	0.0300 ± 0.0090
Human A	Temporal	REM 2	3.6430 ± 0.5540	0.0960 ± 0.1950	0.0320 ± 0.0170
Human B	Temporal	Awake	3.9200 ± 0.7970	0.0080 ± 0.0230	0.0090 ± 0.0070
Human B	Temporal	SWS	3.8950 ± 0.7630	0.0070 ± 0.0140	0.0100 ± 0.0070

Cross species summary of spike avalanche

Table 2. Detailed Awake spike Avalanche

<i>Loc</i>	<i>Bin size(ms)</i>	<i>CDF exponent</i>	<i>Pval</i>	<i>gof</i>
MI	1	2.5	0	0.036
MI	3	5	0.008	0.020
MI	5	3.36	0	0.029
MI	7	3.63	0	0.039
MI	9	3.03	0	0.047
MI	11	3.83	0.327	0.034
MI	13	3.35	0	0.060
MI	15	2.83	0	0.089
PMd	1	4.1	0	0.006
PMd	3	2.81	0	0.021
PMd	5	5	0	0.018
PMd	7	4.85	0.061	0.017
PMd	9	4.03	0	0.022
PMd	11	4.21	0.018	0.024
PMd	13	4.25	0.216	0.019
PMd	15	4.08	0.61	0.017

Monkey A detailed table.

Table 3. Detailed Awake LFP Avalanche

<i>Bin size(ms)</i>	<i>Polarity</i>	<i>Threshold</i>	<i>CDF exponent</i>	<i>Pval</i>	<i>gof</i>
1	neg	Low	1.71	0	0.019
3	neg	Low	2.99	0.056	0.051
5	neg	Low	2.55	0	0.052
7	neg	Low	2.84	0.074	0.052
9	neg	Low	2.42	0	0.053
11	neg	Low	2.37	0	0.059
13	neg	Low	2.43	0	0.054
15	neg	Low	2.36	0	0.052
1	neg	Mid	1.83	0.002	0.015
3	neg	Mid	2.79	0.425	0.040
5	neg	Mid	2.84	0.55	0.042
7	neg	Mid	2.81	0.376	0.048
9	neg	Mid	2.84	0.345	0.050
11	neg	Mid	2.84	0.435	0.048
13	neg	Mid	2.71	0.098	0.058
15	neg	Mid	2.74	0.204	0.056
1	neg	High	1.9	0	0.018
3	neg	High	1.55	0	0.029
5	neg	High	2.44	0.645	0.036
7	neg	High	2.43	0.201	0.046
9	neg	High	2.41	0.672	0.036
11	neg	High	2.39	0.67	0.035
13	neg	High	2.3	0.496	0.036
15	neg	High	2.3	0.36	0.040
1	pos	Low	1.68	0	0.020
3	pos	Low	1.37	0	0.073
5	pos	Low	3.03	0	0.066
7	pos	Low	4.21	0.762	0.051
9	pos	Low	3.59	0.585	0.048
11	pos	Low	3.39	0.43	0.047
13	pos	Low	2.98	0.079	0.046
15	pos	Low	2.9	0.032	0.052
1	pos	Mid	1.74	0	0.018
3	pos	Mid	3.67	0.128	0.062
5	pos	Mid	3.79	0.047	0.069
7	pos	Mid	5	0.827	0.061
9	pos	Mid	3.78	0.797	0.041
11	pos	Mid	3.68	0.926	0.036
13	pos	Mid	3.87	0.797	0.049
15	pos	Mid	3.51	0.553	0.046
1	pos	High	1.76	0.009	0.020
3	pos	High	1.47	0	0.061
5	pos	High	3.19	0.169	0.067
7	pos	High	3.17	0.063	0.066
9	pos	High	3.07	0.251	0.061
11	pos	High	3.09	0.325	0.059
13	pos	High	3.18	0.286	0.062
15	pos	High	2.74	0.033	0.061

Human A detailed Table.